Estimating concentration of toxic ions Arsenic in water by using Photonic Crystal Fiber based on Surface Plasmon Resonance (SPR)

Ghufran Mohammed Jassam *[1,2] iD ✉ , *Soudad S. Ahmed* [2] iD ✉

[1]Al-Farabi University College Department of Optics Techniques, Baghdad Iraq
[2]Department of Physical, College of Science, University of Baghdad, Baghdad Iraq
*Corresponding Author.

Abstract

In this work, an enhanced Photonic Crystal Fiber (PCF) based on Surface Plasmon Resonance (SPR) sensor using a sided polished structure for the detection of toxic ions Arsenic in water was designed and implemented. The SPR curve can be obtained by polishing the side of the PCF after coating the Au film on the side of the polished area, the SPR curve can be obtained. The proposed sensor has a clear SPR effect, according to the findings of the experiments. The estimated signal to Noise Ratio (SNR), sensitivity (S), resolution (R), and Figures of merit (FOM) are approaching; the SNR is 0.0125, S is 11.11 μm/RIU, the resolution is 1.8x 〖10〗 ^(-4), and the FOM is 13.88 for Single-mode Fiber- Photonic Crystal Fiber- single mode Fiber (SMF-PCF-SMF). While the effective performance parameters for Multi-Mode Fiber- Photonic Crystal Fiber- Multi-Mode Fiber (MMF-PCF-MMF) such as the sensitivity is approaching 9.5 μm/RIU, SNR is 0.0173, FOM is10.86 and the resolution is 4x 〖10〗 ^(-4) is achieved. The concentrations were calculated practically and theoretically for each of the sensors, and it was found that the practical concentrations that were obtained are close or equal to the concentrations that were theoretically obtained through the dilution law, where the concentrations were obtained 0.096, 0.15, 0.26, 0.38, 0.49 practically and 0.1, 0.2 and 0 3, 0.4 and 0.5 theoretically For SMF-PCF-SMS, concentrations of 0.089, 0.16, 0.23, 0.34, and 0.45 were practically obtained, and 0.1, 0.2, 0.3, 0.4, and 0.5 theoretically for MMF-PCF-MMF. The suggested sensor has a strong mechanical structure, low cost, and easy fabrication, allowing it to provide a greater measurement range and action area to the measured samples without lengthening the sensor.

Keywords: Arsenic, Mach-Zehnder Interferometer, Photonic Crystal Fiber, Surface Plasmon Resonance, Toxic metal ions.

Introduction

Photonic crystal fibers (PCFs) have grown significantly in recent years due to their distinct microstructures and dispersive properties[1--4]. Microstructure, another name for photonic crystal fibers, is a superior form of optical fiber that has a configuration of air holes running down its length that resembles a crystal lattice[5]. unlike regular single mode fibers, which turn into multimode

below the singlemode cutoff wavelength of each, photonic crystal fibers have the unusual ability to remain single-mode across a large wavelength range. One form of PCF with this capability is the endlessly single-mode fiber (ESM-12) Solid Core Photonic crystal fiber a typical PCF[6]. PCFs are divided into two categories depending on their light-guiding mechanisms: solid core photonic crystal fibers (SC-PCFs), which use a Modified Total Internal Reflection (MTIR) and hollow core photonic crystal fibers (HC-PCFs) which use the Photonic Band Gap (PBG) effect[7]. Surface Plasmon Resonance (SPR) is a very sensitive method for identifying changes in refractive index at the boundary between a metallic layer and a dielectric medium[8,9]. This technology is extensively used as a detecting foundation for many sensors in a number of fields, such as gas sensing, chemical detection, and bio detection[10,11]. Surface Plasmon Resonance, also known as SPR, is an optical phenomenon that happens when light induces a charge density oscillation at the metal dielectric interface by attaining the phase-matching condition between the polarized light and SP[12-15]. PCF-SPR sensors have been created by the integration of plasmatic science and the benefits of photonic crystal fiber technology, and they offer a wide variety of possible uses, including water monitoring[16], environmental surveillance, biochemistry study[17], medical diagnostics, gas detection, and so forth[18]. PCF-SPR uses an evanescent field to create its sensing mechanism. An evanescent field is created when the light of a certain wavelength is shined on the core of the photonic crystal fiber and some of the fields pass into the cladding[19]. The surface Plasmon wave is produced when free electrons in a layer of plasmonic metal, such as silver, gold, aluminum, or copper, interact with evanescent fields. Now that the core guided and SPP modes are connected, a phenomenon known as phase matching has occurred where the core guided mode's refractive index (RI) (real value) is identical to that of the SPP mode[20]. Mach Zehnder Interferometer MZI is among the most often utilized structures in optical and photonic devices. It has been shown that sensors based on the Mach Zehnder Interferometer exist to have an extreme very sensitivity to the medium in which they operate. A typical Mach Zehnder interferometer has

a sensing arm and a reference. A fiber coupler divides the incident light into two arms, which are then recombined by another coupler. The difference in optical pathways between the two arms causes an interference fringe when the two photons join at the second coupler. The reference arm of the MZI is kept apart for ambient refractive index sensing, while the sensor arm is exposed to solutions with varying refractive indices[4]. By examining the alteration in the interference pattern, it is possible to identify the signal deflection in the sensing arm caused by the ambient refractive index changing the optical path variation of the Mach Zehnder Interferometer MZI[21]. In contrast, the 3m of fiber required by the in fiber and coupler-free PCF-MZI indicates a substantially better delay efficiency and offers various advantages, such as compactness and cost savings[22]. The PCFs -Mach Zehnder interferometer is an all-fiber device with enhanced thermal stability and effective optical sensing capabilities [23]. In-fiber free (PCF-MZI) applications are now mostly focused on optical sensing rather than communications, which is the fundamental goal of this effort[24,25]. This work involved the creation and implementation of a Mach-Zehnder mode interferometer for a solid core photonic crystal fiber of endlessly single mode (ESM-12) sensor using a sided polished structure that relies on SPR for the purpose of sensing variations in the refractive index for the toxic metal in ion (Arsenic). The solid core of the PCF sensor's properties has improved due to the coating of a gold layer in the middle of the PCF.

PCF-based interferometry sensors

The Mach Zehnder interferometer MZI, Sagnac interferometer, Fabry Perot interferometer FPI and Michelson interferometer are four examples of interferometry sensing based photonic crystal fiber and their sensor applications. In contrast to traditional optical fibers, PCF structures have a number of desirable characteristics and adjustable qualities that are useful when creating interferometry sensors with improved performance.

Photonic crystal fiber for Endlessly Single mode (ESM-12)

The endlessly single mode solid core photonic crystal fiber a typical PCF, ESM exhibits minimal loss throughout the broadest wavelength range (200 nm to above 2000 nm) while maintaining a nearly constant mode field diameter. The ESM-12 is compatible with all popular fiber tools and has a standard 125 m outside diameter. ESM-12-02 was utilized to produce broadband radiation in a single spatial mode for sensors, interferometers, and short-wavelength applications (visible light and UV). Table.1, lists the ESM-12's physical characteristics (Thorlabs Company).

Table 1. Physical Properties of ESM-12

Physical Properties	
Core measurement	12.2 μm
OD, or outer cladding diameter	125 μm
Size of the coating	245 μm
cladding and core materials	Pure silica
single-layer coating material	Acrylate
Continuity of the coating	< 10 μm
Proving level	0.5 %

Fabrication Mach Zehnder interferometer

When the single light source's incident beam is divided into two arms and then merged to form an interference pattern, the Mach Zehnder interferometer operates. As a result of a problem in one arm, the interference signal fluctuates, changing the optical path length[26]. As shown in Fig (a), a MZI may be made from two fibers, and the light can be separated and recombined using fiber couplers. Two fibers can be used to create a Mach-Zehnder interferometer, and fiber couplers can divide and recombine the light as illustrated in Fig.1 (a). The reference beam is referred to as such, and the detecting beam as such. Making an in line Mach Zehnder interferometer with a single fiber as shown in Fig.1 (b), thus the cladding and core are both coupled to the propagating modes. Even if the two arms are physically the same length, the phase velocity will differ because the clad and core refractive indices are different [27].
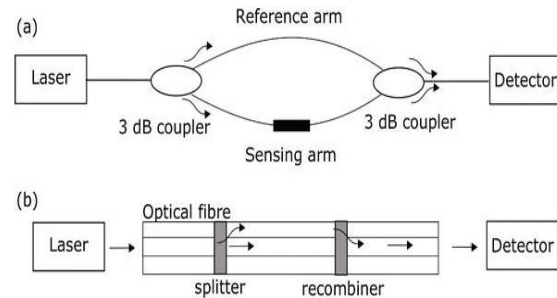
Figure 1. (a) Schematic for a MZI employing two fibers.
(b) Schematic for an in line MZI utilizing a single fiber[27].

Performance Properties

Performance characteristics to be studied include sensitivity, signal to noise ratio, Figure of merit, and resolution. In the case of spectral interrogation, sensitivity can be defined as the change in resonance wavelength per unit change in the refractive index of the sensing medium, and it can be written as[28]:

$$S = \frac{\Delta\lambda_{res}}{\Delta n_s} \qquad \text{……………. 1}$$

Where $\Delta\lambda_{res}$ and Δn_s are the change of the resonance wavelength and the change of refractive index, respectively. From this equation, the unit of sensitivity is nanometers per refractive index unit (nm/RIU).

Signal to noise ratio (SNR) and Fgure of merit (FOM) are inversely proportional to the width of SPR spectral curve and can be written as[28]:

$$\text{SNR (n)} = \left[\frac{\Delta\lambda_{res}}{\Delta\lambda_{0.5}}\right] \qquad \text{………………... 2}$$

Where $\Delta\lambda_{0.5}$ is the width of the spectral curve?

$$FOM = \frac{S}{\Delta\lambda_{0.5}} \qquad \text{………..………… 3}$$

The resolution of the sensor can be defined as the minimum of change in refractive index that is detectable by the sensor, and is given as[29]:

$$R = \frac{\Delta n_s}{\Delta\lambda_{res}} \Delta\lambda_{DR} \qquad \text{………. 4}$$

Where ($\Delta\lambda_{DR}$) is the spectral resolution of the spectrometer.

Experimental Set-up and devices

The setup for estimating toxic ions Arsenic in water based on SPR consist of the following:

Systems using photonic crystal fibers

Solid core endlessly single mode photonic crystal fiber based on a surface plasmon resonance sensor, a D-shaped photonic crystal fiber was built using the ESM-12 SC-PCF. ESM-12 PCF was used for this project because it has the strength to be polished. The characteristics of the PCF are a single mode ESM 12 with cladding diameter of 125 µm and core diameter of 12.2 µm, both made of pure silica. The PCF has two air holes that are each 4.5 µm in diameter (d) and 7.8 µm apart in the center (Λ). The D-shaped PCF, which has flat fiber cladding on top, has drawn interest for SPR sensing. The D-shaped PCF, which has a flat top fiber cladding, has drawn interest for SPR sensing. The metal layer and sample are stacked on top of the flat section of PCFs with the polished portion of the cladding, giving them a D-shape appearance. The placement of a metallic layer close to the core in a D-type PCF allows for strong contact with the sample and an improvement in sensing capability. Fig.2 shows cross section of the D shaped photonic crystal fiber on SPR (a). The distance between the core of the fiber and the side polished flat plane, or polishing depth (h), of 3.8 μm is applied to the upper side of the PCF in order to create a flat surface plane. The coating machine equipment subsequently sputters a 40-nm thick Au coating over the polished surface. A microscope is used to look at the cross section of ESM12-photonic crystal fiber and the side-polished surface of the D shaped PCF, as shown, respectively, in Fig. 2(b) and 2(c). The primary goals of the side polish are to enhance the plasmonic mode and core-guide mode's phase alignment, produce oscillations in the surface plasma, and create a D shaped sensing probe as well as a loss of the main optical field.
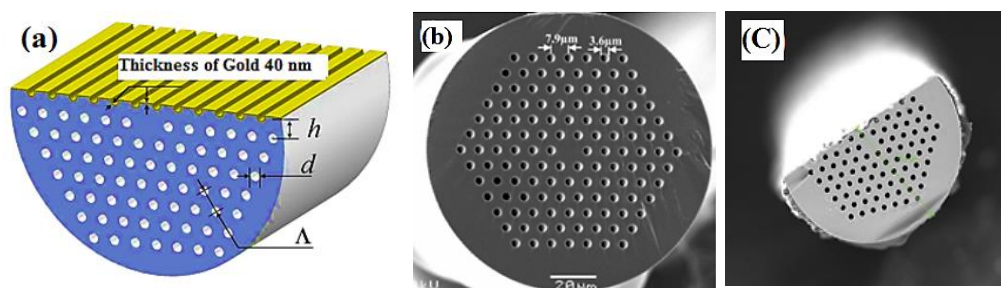
Figure 2. (a) SPR based D shaped PCF cross-section.
(b) SEM image of the PCF taken before polishing.
(c) D shaped for PCF gold-coated cross-section.

Sensor construction with a Mach Zehnder mode interferometer MZI

Mach Zehnder interferometer sensor is built using the SMF-PCF-SMF and MMF-PCF-MMF structures. At the two ends of the sensor, there are single-mode and multi-mode fibers (10μm and 62.5μm core diameters, respectively, and 125μm cladding diameters for both modes). Using a common fusion optical fiber splicer (The Shinho S16) and an optical fiber cleaver, a PCF was inserted between two single mode fibers and multimode fibers in the center of the sensor (Shino X-50C). The PCFs covering layer was removed in order to detect the sensing region. The sensing region was next covered with a 40 nm layer of gold film to achieve the best surface plasmon resonance (SPR) signal using a sputtering coating machine method. Figs. 3 and 4 show single-mode fibre (PCF) and multi-mode fibre (PCF) schematics respectively.
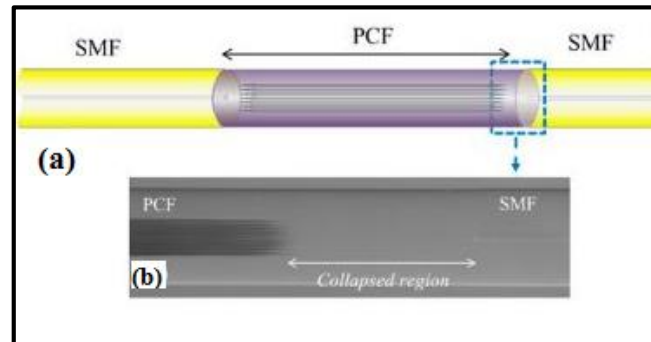
Figure 3. (a) The SMF-PCF-SMF sensor's schematic diagram.
(b) The SMF-PCF fusing splice diagram.
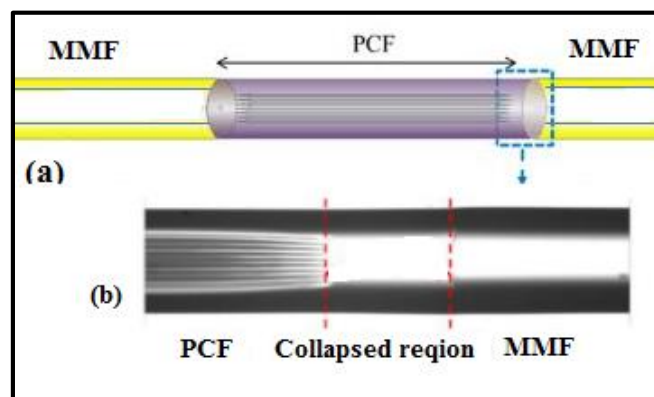
Figure 4. (a) The MMF-PCF-MMF sensor's schematic diagram.
(b) The MMF-PCF fusing splice diagram.

Experimental work

Fig.5, shows the optical setup for SPR-based spectroscopic studies. In the case of SMF-PCF-SMF, is primarily separated into four components. a light beam produced by a HeNe laser with a wavelength of 632 nm with power 0.05mW, PCF (ESM-12) (Thorlabs Co.), Single Mode Fiber, couplers, and a computer-connected spectrophotometer (HR4000CG UV-NIR). While in the case of MMF-PCF- MMF, a halogen lamp light source (DH-2000), PCF (endless single mode-12) (Thorlabs Co.), multi-mode fiber, couplers, and spectrophotometer (HR4000CG UV-NIR) It created many poisonous metal ions (Arsenic) and was connected to a computer. Fig. 5 (a) and (b) show an image of the experimental setup (b).
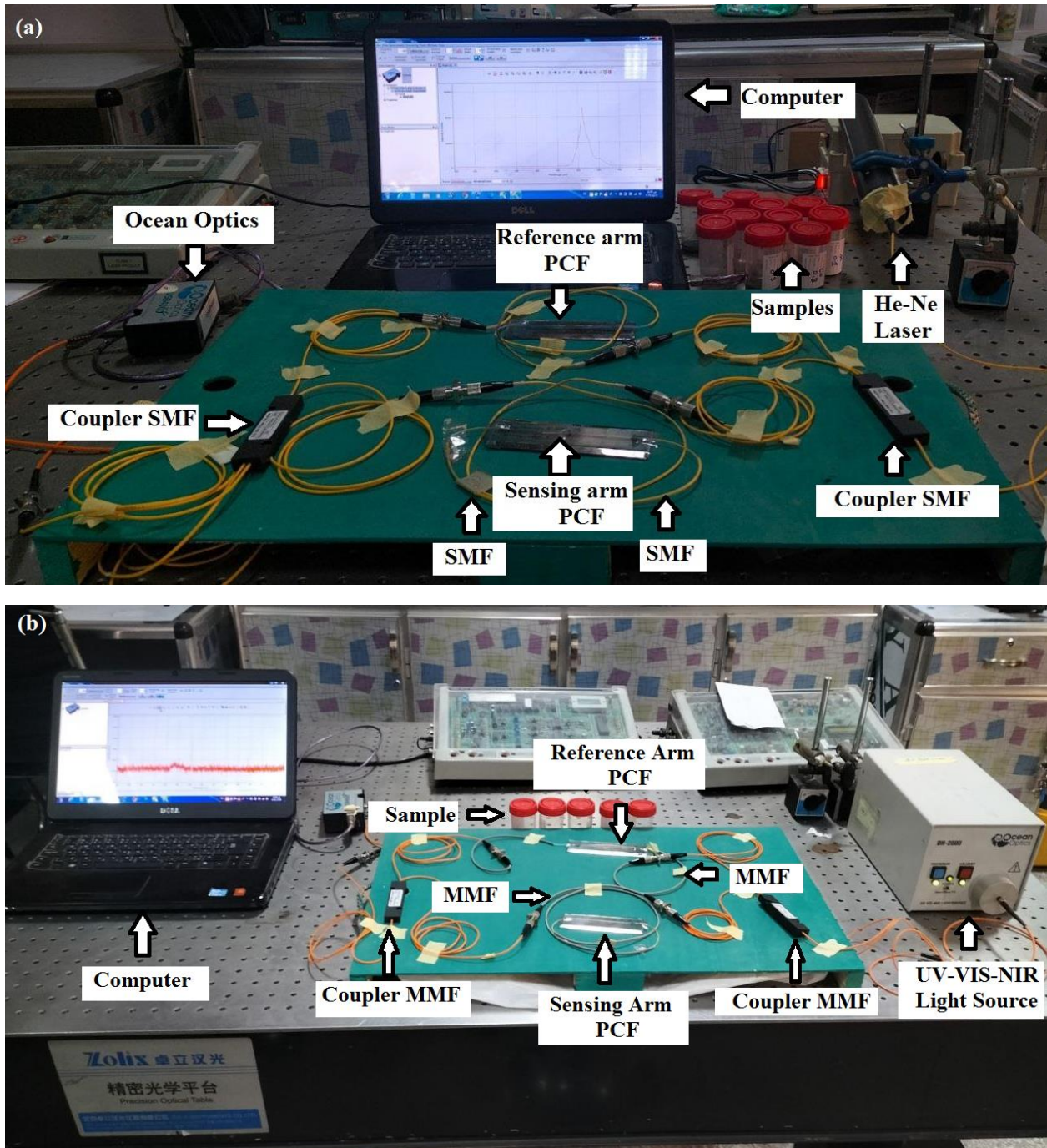
Figure 5. (a) Experimental work of the S PR SMF-PCF-SMF sensor
(b)Experimental work of the S PR SMF-PCF-SMF sensor

Results and Discussion

By immersing the coated middle surface of PCF in the NaCl solution and measuring the solutions' refractive indices, the performance of the sensor is determined. For the sensing technique, a number of solutions were made, and their refractive indices were determined. The calibration curve for SMF-PCF-SMF and MMF-PCF- MMF, as well as the linear connection between refractive index RI and solution concentration, are displayed in Figs. 6 and 7.
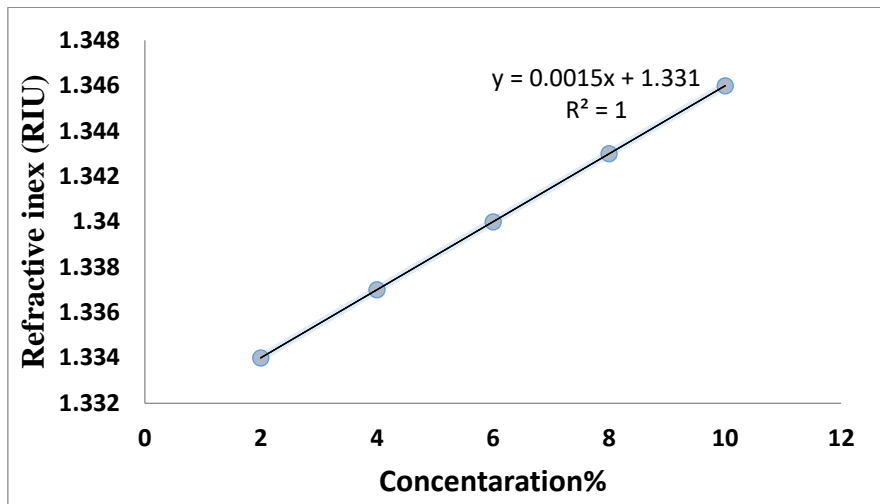
Figure 6. Refractive index via concentration of NaCl solution for SMF-PCF-SMF.
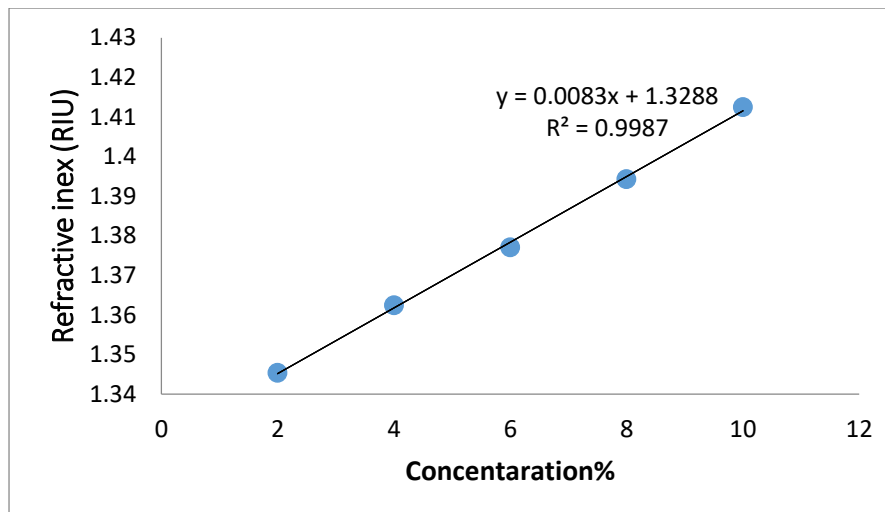
Figure 7. Refractive index via concentration of NaCl solution for multimode fiber-Photonic Crystal Fiber-multimode fiber.

Using a 4 cm long photonic crystal fiber sensor, a coated metal layer (d) thickness of 40 nm, refractive index RI values ranging from (1.334 to 1.346), and a PCF diameter (D) of 125 μm, The sensing process was finished. Figs. 8 and 9 illustrate how the resonance wavelength sharply decreases and shifts toward longer wavelengths (redshift) when the refractive index RI of the sensed area increases. This takes place because the energy decreases and thus the sharp dip of the resonance wavelength will be shifted to the longer wavelength side (red shift), the communication. The spectrum is created by using an optical area to capture light curves. The optical signal intensity (Io) obtained without a sample (sensing area) is divided by the intensity (I)

measured with a sample to determine the transmission (sensing medium). One option is to utilize the transmission as a function of wavelength (nm). The surface plasmon resonance curve is referred to as the resonance wavelength. The wavelength shift, refractive index, and concentration all follow a constant curve relationship. According to Blank's law, which states that the energy is inversely proportional to wavelength, rise in the concentration of toxic metal ions causes an increase in the resonance wavelength, which then causes an increase in the refractive index RI where RIU stands for refractive index unit.
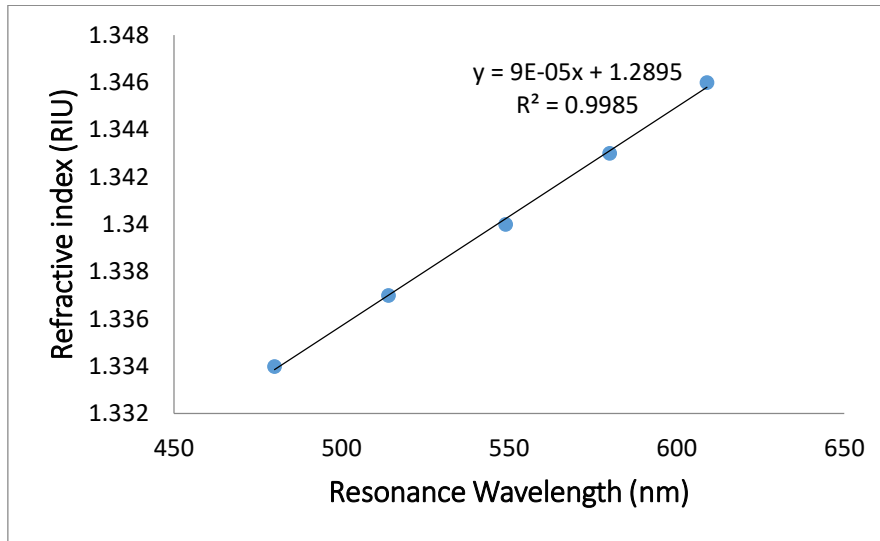
Figure 8. The refractive index as a function resonance wavelength λ_{res} for a gold-coated layer for SMF-PCF-SMF.
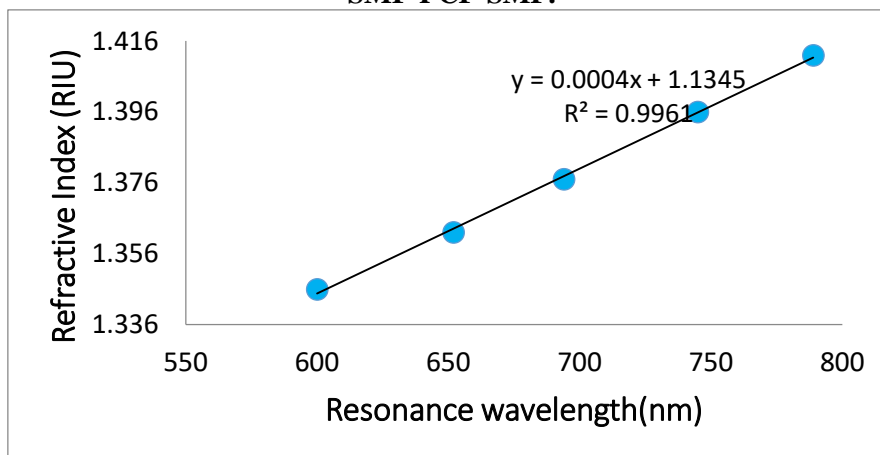
Figure 9.The refractive index as a function resonance wavelength λ_{res} for a gold-coated layer for MMF-PCF-MMF.

The SPR curves for the sensor are displayed in Figs. 10 and 11. As the RI of the arsenic sample varies between 1.34638 and 1.34665, λ_{res} for SMF-PCF-SMF shifts from 632 nm to 635 nm, while the resonance wavelength for multimode fiber-photonic crystal fiber-multimode fiber shifts from 775 nm to 793 nm as the refractive index of the arsenic sample varies between 1.4445 to 1.4517. The SPR response curve demonstrates that each sample has a unique breadth and dip location, or refractive index, which is seen in the change in the regression position for samples containing arsenic. Where (a, b, c, d and e) represent the concentrations that were obtained from Fig. 6 by applying the equation for SMF-PCF-SMF, Y=0.0015X+1.331, while in the case of MMF-PCF-MMF, the equation is Y=0.0083X+1.3288 As in Fig. 7 where y is the refractive index and x is the concentration where this relationship is a constant for measuring the concentrations and refractive indexes of different samples for these sensors.
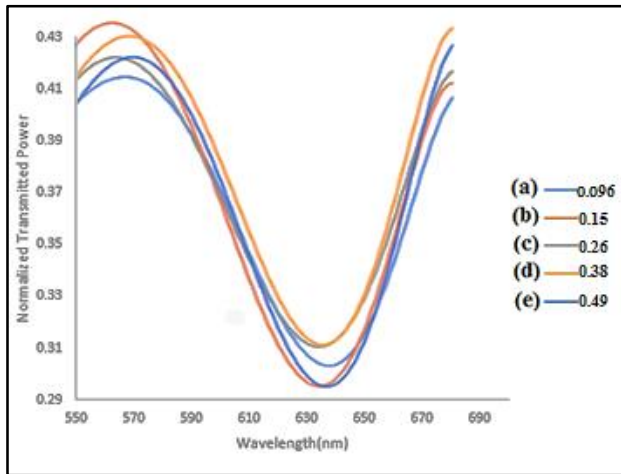
Figure 10. Surface Plasmon Resonance curve for the SMF-PCF-SMF a various of samples of toxic metal ions using gold metal (Arsenic).
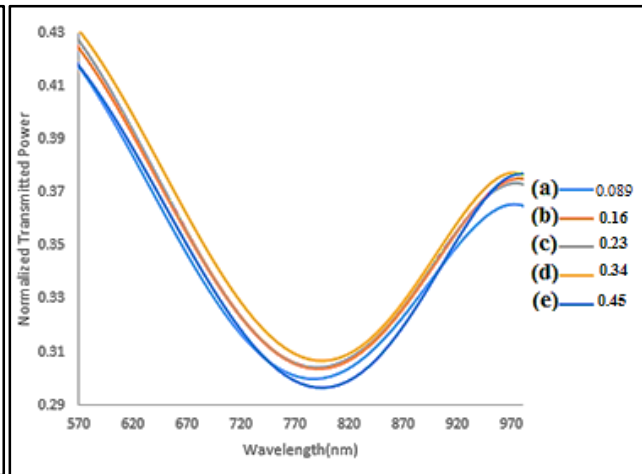
Figure 11. SPR curve of the MMF-PCF-MMF with gold metal for various toxic metal ions samples (Arsenic).

Table. 2, displays the performance parameter of a sensor coated with gold, while Table 3 gives the concentration and refractive index values for each ion toxic Arsenic sample at various resonance wavelengthλ_{res}. Because of the abrupt wavelength variations caused by the red-shift, as the refractive index RI increases, so do the resonance wavelengthsλ_{res} and sample concentration, Where the Concentration of Experiment (C)% represent the concentrations that were obtained from Fig. 6 by applying the equation for SMF-PCF-SMF, Y=0.0015X+1.331, while in the case of MMF-PCF-MMF, the equation is Y=0.0083X+1.3288 as in Fig.7 where y is the refractive index and x is the concentration where this relationship is a constant for measuring the concentrations and refractive indexes of different samples for these sensors. While Concentration of Theory (C) % that was obtained through the dilution law.

Table 2. Performance parameters of gold layer.

Type of fiber	Metal	Sensitivity(S_n) μm/RIU	Signal to noise ratio (SNR)	Figure of merit (FOM)	Resolution (RIU)
SMF-PCF-SMS	Gold	11.11	0.0125	13.88	1.8×10^{-4}
MMF-PCF-MMF	Gold	9.5	0.0173	10.86	4×10^{-4}

Table 3. Concentration sample and refractive index IR values for various arsenicλ_{res}.

Type of fiber	Samples	Resonance wavelength λ_{res} (nm)	Refractive index(RIU)	Concentration of Experiment (C)%	Concentration of Theory (C)%
SMF-PCF-SMS	a	632	1.34638	0.096	0.1
	b	632.5	1.346425	0.15	0.2
	c	633	1.34647	0.26	0.3
	d	634	1.34656	0.38	0.4
	e	635	1.34665	0.49	0.5
MMF-PCF-MMF	a	775	1.4445	0.089	0.1
	b	779	1.4461	0.16	0.2
	c	784	1.4481	0.23	0.3
	d	788	1.4497	0.34	0.4
	e	793	1.4517	0.45	0.5

Conclusion

As the refractive index grows, the resonance wavelength rises (strong shift to the red wavelength) due to an increase in arsenic content in water. Because the sensing medium's refractive index is relatively high, the rear portion of the SP-wave is greater than the imaginary part. As a result, the resonance criterion is met at longer wavelengths. The results show that the optical fiber based on SPR sensing with a 40 nm thickness Au metal layer and 4cm of exposed sensing area achieves effective performance characteristics for SMF-PCF-SMF such as sensitivity reaching 11.11μm/RIU, SNR 0.0125, FOM 13.88, and R is 1.8×10^{-4}, While the performance parameters for multimode fiber - photonic crystal fiber- multimode fiber example sensitivity 9.5μm/RIU, SNR 0.0173, FOM 10.86 and R 4x 10^{-4}.

Author's Declaration

- Conflicts of Interest: None.
- We hereby confirm that all the Figures and Tables in the manuscript are ours. Furthermore, any Figures and images, that are not ours, have been included with the necessary permission for re-publication, which is attached to the manuscript.
- Ethical Clearance: The project was approved by the local ethical committee in University of Baghdad.

Author's Contribution Statement

Gh. M. J.: Drafting the MS, acquisition of data, and analysis. S. S. A.: Supervision, revision, and proof reading. All authors agreed to the final version of this manuscript.

References

1. Jianyang H, Dongying F, Chunli X, Sibang L, Chunlian L, Weimin S, et al. Fiber Mach–Zehnder-interferometer-based liquid crystal biosensor for detecting enzymatic reactions of penicillinase. Appl Opt. 2019 June; 58(17): 4806-4811. https://opg.optica.org/ao/abstract.cfm?uri=ao-58-17-4806
2. Taher HJ. Low loss in Gas filled Hollow core photonic crystal fiber. Baghdad Sci J. 2010 Mar ; 7(1): 129-138. https://doi.org/10.21123/bsj.2010.7.1.129-138
3. Ahsani V, Ahmed F, Jun MBG, Bradley C. Tapered fiber-optic Mach-Zehnder interferometer for ultra-high sensitivity measurement of refractive index. Sensors. 2019 April; 19(7): 1652. https://www.mdpi.com/1424-8220/19/7/1652
4. Salman NA, Taher HJ, Mohammed SA. Tapered Splicing Points SMF-PCF-SMF Structure based on Mach-Zehnder interferometer for Enhanced Refractive Index Sensing. Iraqi J Laser. 2017 Feb; 16(A): 19-24. https://ijl.uobaghdad.edu.iq/index.php/IJL/article/view/41
5. Paul D, Biswas R, Bhattacharyya N. Splicing hetero-core fibers in perspective of different material compositions. Adv Opt Sci Eng. Springer. 2015Jan; 166: 209-214. https://link.springer.com/chapter/10.1007/978-81-322-2367-2_27
6. Flanagan JC, Richardson DJ, Foster MJ, Bakalski I. A microstructured wavefront filter for the Darwin nulling interferometer. Int Conf Space Opt..2006 Nov; 10567: 105672K-1-105672K-9. https://doi.org/110.1117/12.2308141
7. Fatima FA, Soudad SA. Photonic Crystal Fiber Pollution Sensor Based on the Surface Plasmon Resonance Technology. Baghdad Sci J. 2022 Sep: 452-457. https://doi.org/10.21123/bsj.2022.6730
8. Ting Sun, Mengyao Li, Feng Zhao, Lin Liu. Surface plasmon resonance biosensors with magnetic sandwich hybrids for signal amplification. Biosensors. 2022 July; 12(8): 554. https://www.mdpi.com/2079-6374/12/8/554
9. Khatar E, Bassam SS. Surface Plasmon Plastic Optical Fiber Resonance with Multi-Layer as Chemical Sensor. Iraq J Phys. 2021 Sep; 19(50):51-59. https://doi.org/10.30723/ijp.v19i50.588
10. Jabir JN , Areebi NA. High sensitively of double-core surface plasmon resonance biosensor based on photonic crystal fiber. Opt Quant Electron. 2022 Aug; 54(10): 1-18. https://link.springer.com/article/10.1007/s11082-022-03950-y
11. Ghufran MJ,Soudad SA, Murtadha FS. Fabrication of a Chemical Sensor Based on Surface Plasmon

Resonance via Plastic Optical Fiber. *Iraqi J Sci*. 2020 April ; 61(4):765-771. https://doi.org/10.24996/ijs.2020.61.4.8

12. Murtadha FS, Ali AA,Shehab AK. Surface Plasmon Resonance Based Fiber Optic Sensor: Theoretical Simulation and Experimental Realization. ANJS. 2018 Mar; 21(1): 65-70. https://anjs.edu.iq/index.php/anjs/article/view/156/123

13. Jassam GM. Acetic acid concentration estimation using plastic optical fiber sensor based surface plasmon resonance. *Iraq J Phys*. 2019 Nov; 17(43): 11-17. https://ijp.uobaghdad.edu.iq/index.php/physics/article/view/482

14. Namaa SR, Sudad SA, Murtadha FS. Optical Fiber Biomedical Sensor Based on Surface Plasmon Resonance. . *Iraqi J Sci*. 2020 July; 61(7): 1650-1656.https://doi.org/10.24996/ijs.2020.61.7.13

15. Muhammed NF, Mahmood AI, Kadhim SA, Naseef IA. Simulation Design of Hollow Core Photonic Crystal fiber for Sensing Water Quality. J Phys Conf Ser. 2020 May; 1530(1): 12134. https://iopscience.iop.org/article/10.1088/1742-6596/1530/1/012134/meta

16. Maheswaran S, Kuppusamy PG, Ramesh SM, Sundararajan TVP, Yupapin P. Refractive index sensor using dual core photonic crystal fiber–glucose detection applications. Results Phys. 2018 Sep; 11: 577–578. https://doi.org/10.1016/j.rinp.2018.09.055

17. Kawsar A , Bikash KP,Vasudevan B, Ahmed NZR, Maheswar R, Amiri IS , et al.Design of D-shaped elliptical core photonic crystal fiber for blood plasma cell sensing application. Results Phys. 2019 March; 12: 2021–2025. https://doi.org/10.1016/j.rinp.2019.02.026

18. Huizhen Y, Wei J, Shuwen C, Qiang L, Siyu Q, Jianye G, et al. Mercaptopyridine-functionalized gold nanoparticles for fiber-optic surface plasmon resonance Hg^{2+} sensing. ACS Sens. 2019 Feb; 4(3): 704–710. https://doi.org/10.1021/acssensors.8b01558

19. Rahman MT, Sham D, Nazmus MdS. Highly sensitive circular slotted gold-coated micro channel photonic crystal fiber based plasmonic biosensor. OSA Continuum . 2021 May; 4(6): 1808-1826. https://doi.org/10.1364/OSAC.425279

20. Rifat AA, Haider F, Ahmed R, Mahdiraji GA, Adikan FRM, Miroshnichenke E. Highly sensitive selectively coated photonic crystal fiber-based plasmonic sensor. Opt Lett.2018; 43(1): 891-894. https://doi.org/10.1364/OL.43.000891

21. Behrouz BD, Farid JS, Mohsen C.Optoelectronic properties of nanostructured Sb2Se3 films synthesized by electrodeposition method: Effect of Zn concentrations. Sens. Actuator A Phys. 2022 Sep; 344: 113750. https://doi.org/10.1016/j.sna.2022.113750

22. Raisan MT, Tahreer SM. Tunable optical band pass filter using compact Sagnac Fabry perot Hollow core Photonic Crystal Fiber Interferometer. Neuro Quantology. 2022 May; 20(5): 1893-1907. https://www.neuroquantology.com/data-cms/articles/20220606111902am201.pdf

23. Yujian L, Changyuan Y, Ping L. An Optical Fiber Sensor for Axial Strain, Curvature, and Temperature Measurement Based on Single-Core Six-Hole Optical Fiber. Sensors. 2022 Feb; 22(4): 1666. https://www.mdpi.com/1424-8220/22/4/1666

24. Khaleel WA, Al-Janabi A H. Erbium-doped fiber ring laser with wavelength selective filter based on non-linear photonic crystal fiber Mach–Zehnder interferometer. Laser Phys. 2017 Sep; 27(10): 105104. https://iopscience.iop.org/article/10.1088/1555-6611/aa8287/metAa

25. Dora JJH, Zhilin X, Perry PS.Review on photonic crystal fibers with hybrid guiding mechanisms. IEEE Access 2019 May;7: 67469-67482. https://ieeexplore.ieee.org/abstract/document/8719005

26. Marzena H,Daria M,Paweł W,Matthieu W,Mikhael B,Małgorzata JS.Low-coherence interferometric fiber-optic sensors with potential applications as biosensors. Sensors. 2017 Jan; 17(2): 261. https://www.mdpi.com/1424-8220/17/2/261

27. Dora JJH, Rebecca YNW, Perry PS.Photonic crystal fiber-based interferometric sensors. Selected Topics on Optical Fiber Technologies and Applications 2018; 21-41. https://doi.org/10.5772/intechopen.70713

28. Nunzio C, Davide M, Laura C, Luigi Z. Low cost sensors based on SPR in a plastic optical fiber for biosensor implementation. Sensors, 2011 Dec ;11(12): 11752-11760. https://www.mdpi.com/1424-8220/11/12/11752

29. Sachin KS, Banshi DG. Influence of ions on the surface plasmon resonance spectrum of a fiber optic refractive index sensor. Sens Actuator B Chem. 2011Aug; 156(2): 559-562. https://doi.org/10.1016/j.snb.2011.01.068

تقدير تركيز الأيونات السامة الزرنيخ في الماء باستخدام الألياف البلورية الضوئية على أساس رنين البلازمون السطحي(SPR)

غُفران محمد جسام2و1 ، سؤدد سلمان أحمد 1

1اقسم تقنيات البصريات ، كلية الفارابي الجامعة، بغداد ،العراق.
2 قسم الفيزياء، كلية العلوم، جامعة بغداد،بغداد، العراق.

الخلاصة

في هذا العمل ، تم تصميم وتنفيذ ألياف بلورية ضوئية محسنة (PCF) تعتمد على مستشعر رنين البلازمون السطحي (SPR) باستخدام بنية مصقولة من جانب للكشف عن أيونات الزرنيخ السامة في الماء. يمكن الحصول على منحنى SPR عن طريق تلميع جانب PCF بعد طلاء غشاء Auعلى جانب المنطقة المصقولة، ويمكن الحصول على منحنى SPR. المستشعر المقترح له تأثير SPR واضح، وفقًا لنتائج التجارب. تقترب نسبة الإشارة إلى الضوضاء (SNR) والتحسسية (S) و القدرة التحليلية (R) و عامل الجدارة (FOM) ؛ SNR هو 0.0125 ، Sهو μm / RIU 11.11، القدرة التحليلية $1.8x10^{-4}$و، FOM هو 13.88 للألياف أحادية الوضع- الألياف البلورية الضوئية- الألياف أحادية الوضع (SMF-PCF-SMF). في حين أن معلمات الأداء الفعالة للألياف متعددة الأوضاع - الألياف البلورية الضوئية - الألياف متعددة الأوضاع (MMF-PCF-MMF) مثل التحسسية تقترب من 9.5 ميكرومتر μm / RIU ، ، فإن SNR هي 0.0173 ، FOMهي 10.86 و القدرة التحليلية $4x10^{-4}$ تم تحقيقه. تم حساب التراكيز عمليا ونظريا لكل من المتحسسين ووجد ان التراكيز العمليةالتي تم الحصول عليها قريبة او متساوية للتراكيز التي تم الحصول عليها نظريا عن طريق قانون التخفيف حيث تم الحصول على التراكيز 0.096 و 0.15 و0.26و0.38و0.49 عمليا و 0.1و0.2و0.3و0.4و0.5 نظريا للSMF-PCF-SMS وتم الحصول على التراكيز 0.089 و0.16و0.23و 0.34و 0.45 عمليا و0.1و0.2و0.3و0.4و 0.5 نظريا للMMF-PCF-MMFيحتوي المستشعر المقترح على هيكل ميكانيكي قوي ، وتكلفة منخفضة ، وسهولة تصنيع ، مما يسمح له بتوفير نطاق قياس أكبر ومنطقة عمل للعينات المقاسة دون إطالة المتحسس.

الكلمات المفتاحية: الزرنيخ، مقياس التداخل ماخزيندر, الألياف البلورية الضوئية ، رنين البلازمون السطحي ،أيونات المعادن السامة.